UDK 537.622:549.73
Professional article/Strokovni članek

ISSN 1580-2949
MTAEC9, 46(3)305(2012)

STRUCTURAL, THERMAL AND MAGNETIC PROPERTIES OF BARIUM-FERRITE POWDERS SUBSTITUTED WITH Mn, Cu OR Co AND X (X = Sr AND Ni) PREPARED BY THE SOL-GEL METHOD

STRUKTURNE, TERMIČNE IN MAGNETNE LASTNOSTI PRAHOV BARIJEVEGA FERITA, NADOMEŠČENIH Z Mn, Cu ALI Co IN X (X = Sr IN Ni), PRIPRAVLJENIH PO SOL-GEL METODI

Aylin Gurbuz[1], Nurhan Onar[2], Ismail Ozdemir[3], Abdullah Cahit Karaoglanli[3], Erdal Celik[1]

[1]Metallurgical and Materials Engineering Department, Dokuz Eylul University, 35160 Izmir, Turkey
[2]Textile Engineering Department, Pamukkale University, 20020 Denizli, Turkey
[3]Metallurgical and Materials Engineering Department, Bartin University, 74100 Bartin, Turkey
aylingurbuzeng@gmail.com

Prejem rokopisa – received: 2011-10-20; sprejem za objavo – accepted for publication: 2012-02-13

In this study, Ferrite A (undoped barium hexaferrite), Ferrite B (MnCuNi-doped barium hexaferrite), Ferrite C (MnCuSr-doped barium hexaferrite), Ferrite D (MnCoNi-doped barium hexaferrite) and Ferrite E (MnCoSr-doped barium hexaferrite) powders were prepared by sol-gel processing. The produced powders were calcined at 550 °C for 6 h and sintered at 1000 °C for 5 h to obtain the required phases. The powders were characterized by differential thermal analysis/thermogravimetric analysis (DTA/TG), X-ray diffractometry (XRD) and scanning electron microscopy (SEM), and vibrating-sample magnetometry (VSM). The XRD patterns indicated that the pure barium ferrite phase was not obtained. The presence of M-type $BaFe_{11.6}Mn_{0.4}O_{19}$ was confirmed in the Ferrite B and Ferrite D patterns. In the Ferrite C pattern, there were the phases of $BaFe_{12}O_{19}$, $Ba_2Cu_2Fe_{12}O_{22}$ (X or Z-type) and $Sr_3Fe_2O_{6.16}$. The $Ba_{0.5}Sr_{0.5}Fe_{12}$ phase was easily observed in the Ferrite E pattern. The results showed that the dopant materials significantly change the particle shape of Ferrite A powders, but also lower the value of the coercivity. A higher saturation magnetization was observed for the Ferrite D powder.

Keywords: sol-gel, copper-manganese substitution, barium ferrite

V tej raziskavi so prahovi ferita A (nedopiran barijev heksaferit), ferita B (MnCuNi, dopiran barijev heksaferit), ferita C (MnCuSr, dopiran barijev heksaferit), ferita D (MnCoNI, dopiran barijev heksaferit) in ferita E (MnCoSr, dopiran barijev heksaferit) pripravljeni po sol-gel metodi. Prahovi so bili kalcinirani pri 550 °C 6 ur in sintrani pri 1000 °C 5 ur, da so nastale zahtevane faze. Prahovi so bili karakterizirani z diferenčno termično analizo/termogravimetrijsko analizo (DTA/TG), difraktometrijo rentgenskih žarkov (XRD), z vrstičnim elektronskim mikroskopom in z vibracijskih magnetometrom (VSM). XRD-spektri so pokazali, da ni bila dosežena faza čisti barijev ferit. Prisotnost M-tipa $BaFe_{11.6}Mn_{0.4}O_{19}$ je bila potrjena v feritih B in D. V feritu C so bile tudi faze $BaFe_{12}O_{19}$, $Ba_2Cu_2Fe_{12}O_{22}$ (tip X ali Z) in $Sr_3Fe_2O_{6.16}$. Faza $Ba_{0.5}Sr_{0.5}Fe_{12}$ je bila opažena v feritu E. Rezultati so pokazali, da dopanti pomebno spremenijo obliko prahov ferita A in znižajo koercitivnost. Višja magnetna nasičenost je bila opažena pri prahu ferita D.

Ključne besede: sol-gel, substitucija bakra z manganom, barijev ferit

1 INTRODUCTION

Barium hexaferrite powders have been investigated as a material for permanent magnets, microwave absorber devices and recording media[1–7]. Barium hexaferrite is widely used due to its high stability, excellent high-frequency response, narrow switching-field distribution and its temperature coefficient of coercivity in various applications[1,6]. Barium ferrite with a hexagonal molecular structure has a fairly large magnetocrystalline anisotropy, a high Curie temperature and a relatively large magnetization, as well as chemical and corrosion stability[7]. The conventional ceramic methods, i.e., high-energy ball milling and chemical processes such as chemical coprecipitation, the hydrothermal process, the sol-gel process, etc.[8], were employed to obtain high-quality barium ferrite. Wei et al.[9], Wartewig et al.[10], Singh et al.[11], Yadong et al.[12] and Darokar et al.[13] researched the modification of the magnetic parameters of barium ferrite by substitutions[3]. The magnetic properties of barium ferrite could be changed by the substitution of Fe^{+3} with some divalent-tetravalent (Co^{2+}, Ni^{2+}, Ti^{4+}, etc.) metal ions or their combinations, such as Co-Ti, Zn-Ti, Ni-Zr etc[3,14]. Different cation combinations and their different production methods generate different cation distributions and produce different magnetic properties[9]. For example, the saturation magnetization values of Co-Ti-doped barium ferrites slightly decreased with substitutions and their coercivity values rapidly decreased[14–16]. The preparation methods of barium ferrites affect their magnetic and structural properties. The sol-gel method has emerged as a new method for synthesizing barium ferrite for these applications. This method to a large extent determines their homogeneity, particle size, shape and magnetic characteristics[2,17]. In this study, Mn-, Cu- or Co- and Sr, Ni-doped and undoped barium

ferrite nanopowders were produced using sol-gel processing. The thermal, structural, morphological and magnetic properties of the powders were characterized by DTA-TG, XRD, SEM-EDS and VSM, respectively. In addition, the effects of the doping agents on these properties of the barium ferrite powders were investigated.

2 EXPERIMENTAL

2.1 Material and methods

Barium nitrate ($Ba(NO_3)_2$, 99.999 %, Aldrich), ferric citrate mono hydrate ($C_6H_5FeO_7 \cdot H_2O$, 18–20 %, Fluka), manganese (II) nitrate tetrahydrate ($Mn(NO_3)_2 \cdot 4H_2O$, 98.5 %, Merck), copper (II) nitrate trihydrate ($Cu(NO_3)_2 \cdot 3H_2O$, 99–104 %, Fluka), strontium nitrate ($Sr(NO_3)_2$) and nickel(II) nitrate hexahydrate ($Ni(NO_3)_2 \cdot 6H_2O$, 99.999 %, Aldrich), cobalt(II) chloride hexahydrate ($CoCl_2 \cdot 6H_2O$, Sigma-Aldrich) were used as the precursors, citric acid monohydrate ($C_6H_8O_7 \cdot H_2O$, 99.5–100.5 %, Riedel-de Haen) was used as the chelating agent, and ammonium hydroxide (26 %, NH_4OH, Riedel-de Haen) was used as the pH regulator in the production of barium hexaferrite powders. Barium ferrite powders on the atomic scale were prepared by using the citrate sol-gel process. Ferrite A (undoped barium hexaferrite), Ferrite B (MnCuNi-doped barium hexaferrite), Ferrite C (MnCuSr-doped barium hexaferrite), Ferrite D (MnCoNi-doped barium hexaferrite) and Ferrite E (MnCoSr-doped barium hexaferrite) powders were synthesized[3,4]. Stoichiometric amounts of barium nitrate, ferric citrate, manganese nitrate tetrahydrate, citric acid, copper (II) nitrate trihydrate or cobalt(II) chloride hexahydrate were used to produce the main phase including MnCu- (Ferrite B and Ferrite C) or MnCo- (Ferrite D and E) doped barium ferrites. The barium nitrate and ferric citrate were dissolved in the citric acid solution. The ratios of citric acid: metal = 3 and Fe:Ba = 11 were used from Ref. 1 and 10. Both solutions were mixed. The manganese nitrate, copper (II) nitrate trihydrate, cobalt (II) chloride hexahydrate, strontium nitrate and nickel(II) nitrate hexahydrate were subsequently added to the solution as doping agents in stoichiometric ratios. These solutions were vigorously mixed with a magnetic stirrer until a transparent solution was obtained. Ammonium hydroxide was added to the solution until a pH value of 7.0 was attained at room temperature and then the solution was stirred with a magnetic stirrer. Thus, it was designed to acquire homogeneity in the suspension and stability of pH in the solution during whole solution-preparation process[1,18]. The solution was kept in a water bath at 80 °C for 15 h. The water in the solution was then gradually removed and a wet gel with high viscosity was obtained.

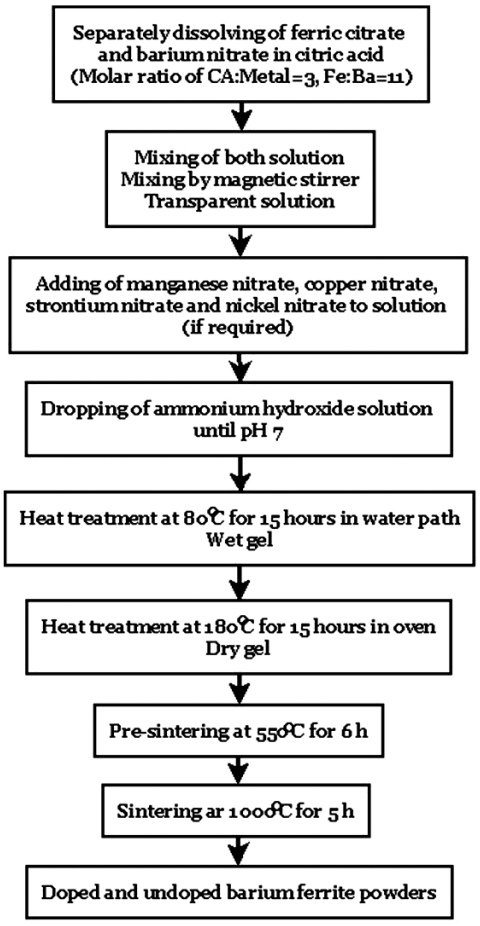

Figure 1: The flow chart of sol-gel citrate process to produce barium ferrite powders

Slika 1: Shema sol-gel citratnega procesa za izdelavo prahov barijevega ferita

The wet gel was treated at 180 °C for 15 h in a Nüve KD400 oven (Nüve, Inc., Ankara, Turkey) to prepare a dry gel. The dry gel was exposed to a pre-sintering process at 550 °C for 6 h to evaporate any impurities and then sintered at 1000 °C for 5 h in ash oven in air[19,2]. The produced powders were characterized by using DTA-TG, XRD, SEM and VSM. The flow chart of the sol-gel citrate process to produce the barium ferrite powders is shown in **Figure 1**.

2.2 Characterization

To determine the decomposition and phase formation of barium ferrite powders, which were dried at 180 °C for 15 h in air, their thermal behavior was evaluated with a DTA–TG device (DTG-60H, Shimadzu, Kyoto, Japan) at a heating rate of 10 °C/min at a temperature range of 0–1200 °C under an oxygen atmosphere.

In order to identify the phase structure, XRD patterns of the barium ferrite powders were determined by means of a Rigaku D Max-2200/PC X-ray diffractometer (Rigaku Corp., Tokyo, Japan) with CuK_α irradiation (wavelength, $\lambda = 0.15418$ nm) using both the θ–2θ mode and the 2θ scan mode. The diffracted X-ray beam was collected by scanning the detector between $2\theta = 3°$ and 90°. The surface morphologies of the barium ferrite powders were examined with a JEOL JJM 6060 scanning electron microscope attached to an energy-dispersive spectroscopy apparatus (JEOL Ltd., Tokyo, Japan). The

magnetic properties of the barium ferrite powders were measured at room temperature on a vibrating-sample magnetometer (VSM, Lakeshore 736, 7400 Series) in a maximum applied field of 15,000 Gauss. From the obtained hysteresis loops, the saturation magnetization (M_s) and coercivity (H_c) were determined.

3 RESULTS AND DISCUSSION

3.1 DTA-TG-analysis

The thermal behavior of the Ba- and Fe-based xerogel powder samples, which were dried at 180 °C for 6 h in air, was evaluated at a heating rate of 10 °C/min in an oxygen atmosphere by DTA/TG analysis in order to determine the temperature of the decomposition and phase formation, and to obtain an optimum heat-treatment regime. **Figure 2** and **3** demonstrate the DTA and TG curves of Ferrite A ($BaFe_{12}O_{19}$), Ferrite B ($BaFe_{12-x}(Mn_{0.5}Cu_{0.5}Ni)_{x/2}O_{19}$)), Ferrite C ($BaFe_{12-x}(Mn_{0.5}Cu_{0.5}Sr)_{x/2}O_{19}$)), Ferrite D ($BaFe_{12-x}(Mn_{0.5}Co_{0.5}Ni)_{x/2}O_{19}$)) and Ferrite E ($BaFe_{12-x}(Mn_{0.5}Co_{0.5}Sr)_{x/2}O_{19}$)) powders for x = 2. In **Figure 2**, the endothermic peaks between 70 °C and 100 °C were due to the removal of solvents in their nature and the endothermic peaks between 200 °C and 300 °C were the result of the degradation of carbon-based organic matter due to the precursors materials, chelating agents and solvents. The exothermic peak between 600 °C and 700 °C resulted from a pure, barium ferrite phase transformation[20].

Moreover, the TG analysis gives the results of the weight loss of the powder samples in the temperature range 0–1200 °C in **Figure 3**. As seen in **Figure 3**, the weight losses of Ferrite A ($BaFe_{12}O_{19}$), Ferrite B ($BaFe_{12-x}(Mn_{0.5}Cu_{0.5}Ni)_{x/2}O_{19}$)), Ferrite C ($BaFe_{12-x}(Mn_{0.5}Cu_{0.5}Sr)_{x/2}O_{19}$)), Ferrite D ($BaFe_{12-x}(Mn_{0.5}Co_{0.5}Ni)_{x/2}O_{19}$)) and Ferrite E ($BaFe_{12-x}(Mn_{0.5}Co_{0.5}Sr)_{x/2}O_{19}$)) powders were, respectively, 76 %, 42 %, 33 %, 30 % and 28 %, for temperatures ranging from 0 °C to 1200 °C. In this range of thermal treatment, the weight loss was a result of the solvent removal and the combustion of carbon-based materials. The weight loss up to 200 °C was a small amount since that loss was due to solvent removal. The removal of organic materials up to 300 °C resulted in larger weight loss. The weight loss observed between 600 °C and 800 °C could be the result of Mn or Cu evaporation[21,22].

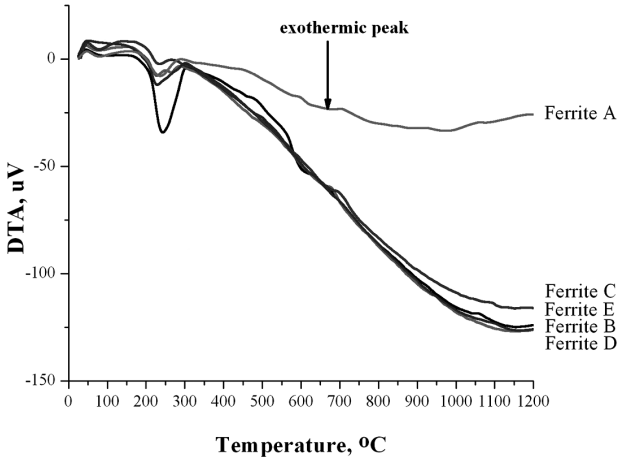

Figure 2: The DTA curves of the Ferrite A ($BaFe_{12}O_{19}$), Ferrite B ($BaFe_{12-x}(Mn_{0.5}Cu_{0.5}Ni)_{x/2}O_{19}$)), Ferrite C ($BaFe_{12-x}(Mn_{0.5}Cu_{0.5}Sr)_{x/2}O_{19}$)), Ferrite D ($BaFe_{12-x}(Mn_{0.5}Co_{0.5}Ni)_{x/2}O_{19}$)) and Ferrite E ($BaFe_{12-x}(Mn_{0.5}Co_{0.5}Sr)_{x/2}O_{19}$)) powders

Slika 2: DTA-krivulje prahov ferita A ($BaFe_{12}O_{19}$), ferita B ($BaFe_{12-x}(Mn_{0,5}Cu_{0,5}Ni)_{x/2}O_{19}$)), ferita C ($BaFe_{12-x}(Mn_{0,5}Cu_{0,5}Sr)_{x/2}O_{19}$)), ferita D ($BaFe_{12-x}(Mn_{0,5}Co_{0,5}Ni)_{x/2}O_{19}$)) in ferita E ($BaFe_{12-x}(Mn_{0,5}Co_{0,5}Sr)_{x/2}O_{19}$))

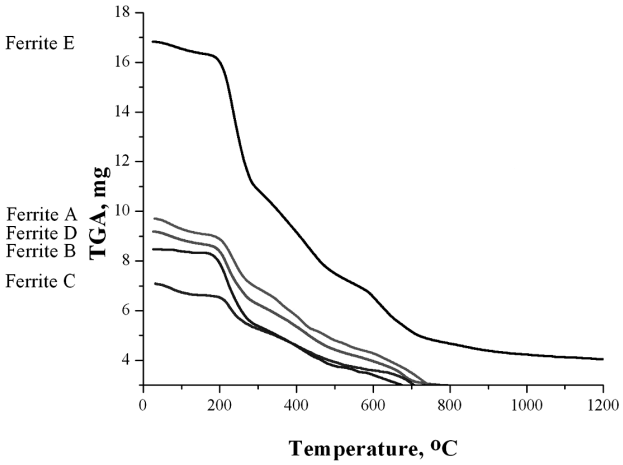

Figure 3: The TG curves of the Ferrite A ($BaFe_{12}O_{19}$), Ferrite B ($BaFe_{12-x}(Mn_{0.5}Cu_{0.5}Ni)_{x/2}O_{19}$)), Ferrite C ($BaFe_{12-x}(Mn_{0.5}Cu_{0.5}Sr)_{x/2}O_{19}$)), Ferrite D ($BaFe_{12-x}(Mn_{0.5}Co_{0.5}Ni)_{x/2}O_{19}$)) and Ferrite E ($BaFe_{12-x}(Mn_{0.5}Co_{0.5}Sr)_{x/2}O_{19}$)) powders

Slika 3: TG-krivulje prahov ferita A ($BaFe_{12}O_{19}$), ferita B ($BaFe_{12-x}(Mn_{0.5}Cu_{0.5}Ni)_{x/2}O_{19}$)), ferita C ($BaFe_{12-x}(Mn_{0.5}Cu_{0.5}Sr)_{x/2}O_{19}$)), ferita D ($BaFe_{12-x}(Mn_{0,5}Co_{0,5}Ni)_{x/2}O_{19}$)) in ferita E ($BaFe_{12-x}(Mn_{0,5}Co_{0,5}Sr)_{x/2}O_{19}$))

The exothermic and endothermic reactions occur in the temperature range of about 70 °C to 1200 °C. There are four different steps, including the removal of solvent-based materials, the combustion of carbon-based content, the formation of oxides and barium hexaferrite. The procedure of heat treatment to produce barium ferrite powder was determined according to the DTA-TG results. As a result of that, the xerogel was treated at 80 °C for 15 h to remove water and then treated to produce a dry gel at 180 °C for 15 h in an oven. Subsequently, the powders were sintered at 550 °C for 6 h and at 1000 °C for 5 h for transforming the oxide form and then the ferrite form, respectively. It was reported that the high values of coercivity and magnetic saturation are linked to the annealing temperature. Annealing at higher temperatures led to an increase in the crystallite size and resulted in a decrease of the coercivity[23].

3.2 XRD-analysis

Figure 4 shows XRD patterns of the Ferrite A ($BaFe_{12}O_{19}$), Ferrite B ($BaFe_{12-x}(Mn_{0.5}Cu_{0.5}Ni)_{x/2}O_{19}$)), Ferrite C ($BaFe_{12-x}(Mn_{0.5}Cu_{0.5}Sr)_{x/2}O_{19}$)), Ferrite D

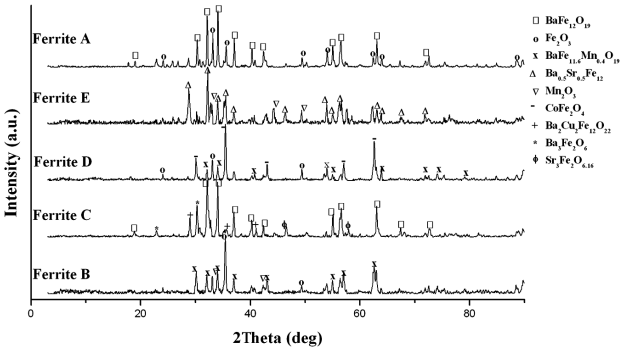

Figure 4: XRD patterns of the Ferrite A ($BaFe_{12}O_{19}$), Ferrite B ($BaFe_{12-x}(Mn_{0.5}Cu_{0.5}Ni)_{x/2}O_{19}$)), Ferrite C ($BaFe_{12-x}(Mn_{0.5}Cu_{0.5}Sr)_{x/2}O_{19}$)), Ferrite D ($BaFe_{12-x}(Mn_{0.5}Co_{0.5}Ni)_{x/2}O_{19}$)) and Ferrite E ($BaFe_{12-x}(Mn_{0.5}Co_{0.5}Sr)_{x/2}O_{19}$)) powders

Slika 4: XRD-spektri prahov ferita A ($BaFe_{12}O_{19}$), ferita B ($BaFe_{12-x}(Mn_{0,5}Cu_{0,5}Ni)_{x/2}O_{19}$)), ferita C ($BaFe_{12-x}(Mn_{0,5}Cu_{0,5}Sr)_{x/2}O_{19}$)), ferita D ($BaFe_{12-x}(Mn_{0,5}Co_{0,5}Ni)_{x/2}O_{19}$)) in ferita E ($BaFe_{12-x}(Mn_{0,5}Co_{0,5}Sr)_{x/2}O_{19}$))

($BaFe_{12-x}(Mn_{0.5}Co_{0.5}Ni)_{x/2}O_{19}$)) and Ferrite E ($BaFe_{12-x}(Mn_{0.5}Co_{0.5}Sr)_{x/2}O_{19}$)) powders produced by the sol-gel citrate process.

The pure barium ferrite phase was not obtained. The presence of the barium ferrite phase and also the small amount of iron oxide (Fe_2O_3) phase in the pattern can be observed in the powders in **Figure 4**. Zhong et al.[24] reported that preheating the gel, which is prepared by sol-gel process, to 400–500 °C prevented any α-Fe_2O_3 phases from forming in the barium ferrite structure. In this study, the presence of the Fe_2O_3 phase was observed in the structure, despite the preheating process, which was conducted at 500 °C for 6 h. The presence of the M-type of $BaFe_{11.6}Mn_{0.4}O_{19}$ was confirmed in the Ferrite B and Ferrite D patterns. In these patterns, the dominant crystalline phase was $BaFe_{11.6}Mn_{0.4}O_{19}$. Thus, we observed the presence of Mn in the barium ferrite structure. This means that the manganese dissolved in the barium ferrite structure and the solid reaction was heterogeneous[20]. It was also determined that the iron substituted with the Mn and the element was embedded in the barium ferrite structure in the $BaFe_{11.6}Mn_{0.4}O_{19}$ form. The existence of phases other than those mentioned above was also observed in the structure. The sol-gel method is an appropriate process for the preparation of multicomponent oxides at relatively low temperatures. The sol-gel process aids not only in reducing the application temperature of the heat treatment but also in controlling the homogeneity and the microstructure. In this study, the XRD patterns obtained were generally complicated and have indicated various phases in the structures. This means the XRD patterns were in agreement with the literature[25]. The Ferrite C pattern indicated phases of $BaFe_{12}O_{19}$, $Ba_2Cu_2Fe_{12}O_{22}$ (X or Z- type) and $Sr_3Fe_2O_{6.16}$. In the pattern the Sr was replaced with Ba and Mn, and the Cu was replaced with Fe, in accordance with Ref. [26]. In the Ferrite D pattern, it was observed that the $CoFe_2O_4$ phase was the dominant phase. In the material, Co was completely substituted by barium. $CoFe_2O_4$ is one of the well-known hard magnetic materials with a very high cubic magnetocrystalline anisotropy, high coercivity, average magnetic saturation[27]. As a result of that, the iron was substituted with manganese and copper in M-type hexagonal ferrites, such as $BaFe_{12}O_{19}$ [28]. Hexagonal ferrites produced have different types, such as the M-, W-, Z- and Y-types, which have complex crystal and magnetic structures. It was also reported in the literature that the magnetic ions can be removed by replacing them with divalent ions[29,30]. It was also reported that magnetic ions can be removed by replacing them with divalent ions[29,30].

3.3 SEM-analysis

The average grain size and the shape of Ferrite A (undoped barium hexaferrite), Ferrite B (MnCuNi-doped barium hexaferrite), Ferrite C (MnCuSr-doped barium hexaferrite), Ferrite D (MnCoNi-doped barium hexaferrite) and Ferrite E (MnCoSr-doped barium hexaferrite) powders are shown in **Figures 5a, 5b, 5c, 5d** and **5e**, respectively. The Ferrite A powders with a platelet microstructure can be seen in **Figure 5a**. This indicates that the M-type ferrite grains are hexagonal-shaped crys-

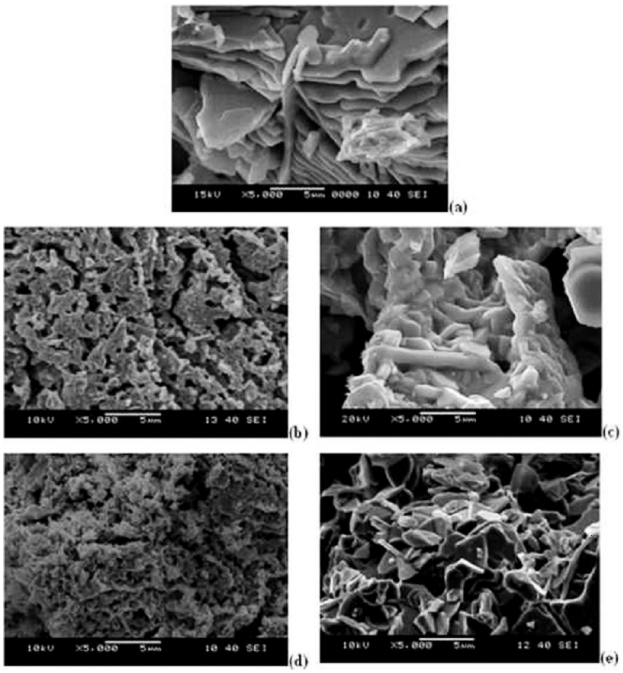

Figure 5: The SEM images of: a) Ferrite A (undoped barium hexaferrite), b) Ferrite B (MnCuNi-doped barium hexaferrite), c) Ferrite C (MnCuSr-doped barium hexaferrite), d) Ferrite D (MnCoNi-doped barium hexaferrite) and e) Ferrite E (MnCoSr-doped barium hexaferrite) powders

Slika 5: SEM-posnetki: a) ferit A (nedopiran barijev heksaferit), b) ferit B (MnCuNi, dopiran barijev heksaferit), c) ferit C (MnCuSr, dopiran barijev heksaferit), d) ferit D (MnCoNi, dopiran barijev heksaferit) in e) ferit E (MnCoS, dopiran barijev heksaferit)

tals. The critical diameter of the spherical barium ferrite with a single magnetic domain is reported to be 460 nm.

Since the produced powders were sintered at 1000 °C, single barium hexaferrite particles were observed in this study. This is why grain growth occurs during the sintering process as well as agglomeration during the preparation of the powders. Similar behavior has been observed previously[2]. **Figure 5d** shows a typical morphology of Ferrite D powders. The major microstructure of Ferrite D powders resembles sponge. The microstructures of the Ferrite C powders were commonly hexagonal shaped (**Figure 5c**). The Ferrite B powders seem to mostly agglomerate, but also the microstructure seems to have a hexagonal shape, as seen in **Figure 5b**. In the microstructure of the Ferrite E powder, the hexagonal shape is the major structure (see **Figure 5e**).

3.4 VSM-analysis

Figure 6 shows the hysteresis curves of $BaFe_{12}O_{19}$ provided by the Aldrich company, Ferrite A (undoped barium hexaferrite), Ferrite B (MnCuNi-doped barium hexaferrite), Ferrite C (MnCuSr-doped barium hexaferrite), Ferrite D (MnCoNi-doped barium hexaferrite) and Ferrite E (MnCoSr-doped barium hexaferrite) powders. Moreover, the magnetic saturation and coercivity values of these powders are given in Table 1. The coercivity value of the Ferrite A powder was 214.859 kA/m (2700 Oe). This value was lower than the value of the $BaFe_{12}O_{19}$ powder provided by the Aldrich company, which was 294.436 kA/m (3700 Oe). It was determined that the magnetic saturation values of the Ferrite A and the $BaFe_{12}O_{19}$, which was provided by Aldrich company, were 55.64 and 34.38 emu/g, respectively. As a result of that, the materials have ferromagnetic properties. It is possible that the higher magnetic saturation values of the Ferrite A powder resulted from agglomerated particles.

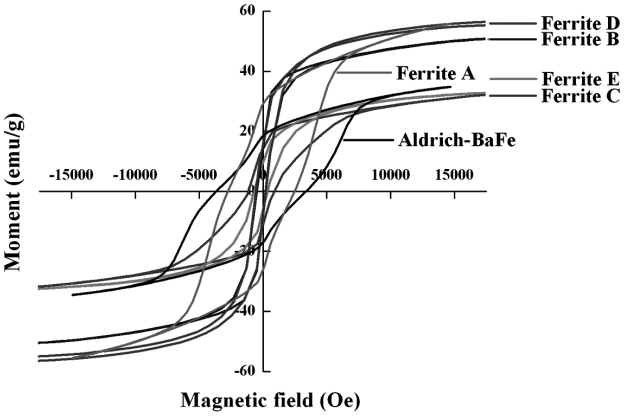

Figure 6: The hysteresis curves of $BaFe_{12}O_{19}$ provided by the Aldrich Company: Ferrite A (undoped barium hexaferrite), Ferrite B (MnCuNi-doped barium hexaferrite), Ferrite C (MnCuSr-doped barium hexaferrite), Ferrite D (MnCoNi-doped barium hexaferrite) and Ferrite E (MnCoSr-doped barium hexaferrite) powders

Slika 6: Histerezne krivulje prahov $BaFe_{12}O_{19}$ od družbe Aldrich: ferit A (nedopiran barijev heksaferrit), ferit B (MnCuBNi, dopiran barijev heksaferit), ferit C (MnCuSr, dopiran barijev heksaferit), ferit D (MnCoNi, dopiran barijev heksaferit) in ferit E (MnCoSr, dopiran barijev heksaferit)

Table 1: The magnetic saturation and coercivity values of $BaFe_{12}O_{19}$ provided by the Aldrich Company: Ferrite A (undoped barium hexaferrite), Ferrite B (MnCuNi-doped barium hexaferrite), Ferrite C (MnCuSr-doped barium hexaferrite), Ferrite D (MnCoNi-doped barium hexaferrite) and Ferrite E (MnCoSr-doped barium hexaferrite) powders.

Tabela 1: Magnetna nasičenost in koercitivna sila $BaFe_{12}O_{19}$ iz družbe Aldrich: ferit A (nedopiran barijev heksaferrit), ferit B (MnCuBNi, dopiran barijev heksaferit), ferit C (MnCuSr, dopiran barijev heksaferit), ferit D (MnCoNi, dopiran barijev heksaferit) in ferit E (MnCoSr, dopiran barijev heksaferit)

Materials	Magnetic Saturation (emu/g)	Coercivity (kA/m)
Purchased nanopowder (Aldrich)	34.38	294.436
Ferrite A powder	55.64	214.859
Ferrite B powder	50.68	27.836
Ferrite C powder	32.07	82.466
Ferrite D powder	55.16	30.304
Ferrite E powder	32.66	42.472

As seen in **Table 1**, the coercivity values of the barium ferrite powders doped with different divalent metals decreased and the magnetic properties approached superparamagnetic properties. In particular, the magnetic saturation values with nickel doping to barium ferrite powders were high, while the magnetic saturation values with strontium doping were low.It is reported that undoped hexaferrite possesses a very high coercive force, which is due to its uniaxial anisotropy along the c-axis of the M-type hexaferrite. In our study, Mn-Cu-Co-Ni-Sr substitution led to a significant decrease of H_c compared to the reported Hc value for the undoped hexaferrite, owing to a reduction of the magnetocrystalline anisotropy. Similar results were also reported for Mn-Co-Ti-substituted barium ferrites by Ghasemi et al.[2] and for Mg-Ti-substituted barium ferrite by Shams et al.[31]. It is believed that the coercivity of the doped hexaferrite was low compared to the coercivity of the undoped barium hexaferrite powders because of the change in the easy axis of magnetization from the c-axis to the basal plane[31]. Ghasemi et al.[2] advocated the results that were indicated by Shams et al.[31]. Tech et al.[26] pointed out that Co(II) substitution in $BaFe_{12}O_{19}$ reduced the coercivity from 1082 G mg^{-1} to 275.8 G mg^{-1}. The hysteresis loss area in the cobalt (II)-substituted barium hexaferrite is smaller than the undoped one.

4 CONCLUSIONS

Ferrite A (undoped barium hexaferrite), Ferrite B (MnCuNi-doped barium hexaferrite), Ferrite C (MnCuSr-doped barium hexaferrite), Ferrite D (MnCoNi-doped barium hexaferrite) and Ferrite E (MnCoSr-doped barium hexaferrite) powders were prepared by using a citrate sol-gel process. The heat-treat-

ment regimes of the powders were determined according to the DTA-TG results. The dopant materials significantly influenced the microstructure of the Ferrite A powder. In particular, the addition of the Sr dopant to barium ferrite powders had a significant role in the production of powders with a hexagonal microstructure. The VSM results are in reasonable agreement with the literature. The doping elements decreased the coercivity of these powders. As the coercivity values of Ferrite A powders were larger than the doped powders, the coercivity value was found about 214.859 kA/m (2700 Oe) for Ferrite A powders and was changed from about 27.285 kA/m (349.8 Oe) and 82.466 kA/m (1036.3 Oe) for the doped barium hexaferrite powders. The XRD results showed that the Ferrite powders produced by the sol-gel process contained a small amount of iron oxide (Fe_2O_3) in their structure in addition to the barium ferrite phase. For doped barium ferrite powders, the iron was substituted with manganese and copper in M-type hexagonal ferrites, such as Ferrite A, while the Sr element was replaced by the Ba element. In conclusion, the dissolution of the Mn, Cu and Sr elements in the Ferrite A structure at the atomic level was successfully accomplished by the sol-gel process.

Acknowledgements

The study has been supported by The Scientific and Technological Research Council of Turkey (TUBITAK, 106M391).

5 REFERENCES

[1] Z. Haijun, L. Zhichao, M. Chengliang, Y. Xi, Z. Liangying, W. Mingzhong, Mater. Sci. Eng. B, 96 (**2002**), 289–295
[2] A. Ghasemi, A. Saatchi, M. Salehi, A. Hossienpour, A. Morisako, X. Liu, Phys Status Solidi A, 10 (**2006**), 2513–2521
[3] Z. Haijun, L. Zhichao, M. Chengliang, Y. Xi, Z. Liangying, W. Mingzhong, Mater Chem Phys., 80 (**2003**), 129–134
[4] G. Mendoza-Suarez, L. P. Rivas- Vazquez, J. C. Corral-Huacuz, A. F. Fuantes, J. I. Escalante-Garcia, Physica B, 339 (**2003**), 110–118
[5] H. Hua, S. Z. Li, Z. D. Han, D. H. Wang, M. Lu, W. Zhong, B. X. Gu, Y. W. Du, Mat. Sci. Eng A-Struct, 448 (**2007**), 326–329
[6] G. Mendoza-Suarez, L. P. Rivas- Vazquez, A. F. Fuantes, J. I. Escalante-Garcia, O. E. Ayala-Valenzuela, E. Valdez, Mater. Lett., 57 (**2002**), 868–872
[7] J. Zhou, H. Ma, M. Zhong, G. Xu, Z. Yue, Z. He, J Magn Magn Mater., 305 (**2006**), 467–469
[8] P. Sharma, R. A. Rocha, S. N. de Medeiros, A. Paesano Jr, J Alloy Compds., 443 (**2007**), 37–42
[9] F. L. Wei, H. C. Fang, C. K. Ong, et al., J. Appl. Phys., 87 (**2000**), 8636–8639
[10] P. Wartewig, M. K. Krause, P. Esquinazi et al., J. Magn. Magn. Mater., 192 (**1999**), 83–99
[11] P. Singh, V. K. Babbar, A. Razdan et al., Mater. Sci. Eng. B, 67 (**1999**), 132–138
[12] L. Yadong, L. Renmao, Z. Zude et al., Mater. Chem. Phys., 64 (**2000**), 256–259
[13] S. S. Darokar, K. G. Rewatkar, D. K. Kulkarni, Mater. Chem. Phys., 56 (**1998**), 84–86
[14] Z. W. Li, C. K. Ong, Z. Yang, F. W. Wei, X. Z. Zhou, J. H. Zhao, A. H. Morrish, Phys. Rev. B, 62 (**2000**), 6530–6537
[15] O. Kubo, T. Ido, and H. Yakoyama, IEEE Trans. Magn. 18 (**1982**), 1122
[16] Z. Yang, J. H. Zhao, H. X. Zeng, G. Yan, Int. J. Soc. Mater. Eng. Resour., 3 (**1995**), 203
[17] A. Mali, A. Ataie, Ceram Int., 30 (**2004**), 1979–1983
[18] L. Dong, Z. Han, Y. Zhang, Z. Wu, Z. Zhang, Rare Metals, 25 (**2006**), 605–608
[19] A. Ghasemi, X. Liu, A. Morisako, J Magn Magn Mater., 316 (**2007**), e105–e108
[20] O. Carp, R. Barjega, E. Segal, M. Brezeanu, Thermochim Acta, 318 (**1998**), 57–62
[21] A. Hakola, O. Heczko, A. Jaakkola, T. Kajava, K. Ullakko, Appl Phys A, 79 (**2004**), 1505–1508
[22] S. T. Park, W. Kang, H. T. Kim, S. J. Yun, B Korean Chem Soc., 293 (**2008**), 685–688
[23] J. Ding, W. F. Miao, P. G. McCormick, R. Street, J Alloy Compd., 281 (**1998**), 32–36
[24] W. Zhong, W. Ding, N. Zhang, J. Hong, Q. Yan, Y. Du, J Magn Magn Mater., 168 (**1997**), 196–202
[25] N. C. Pramanik, T. Fujii, M. Nakanishi, J. Takada, S. I. Seok, Mater Lett., 60 (**2006**), 2718–2722
[26] G. B. The, S. Nagalingam, D. A. Jefferson, Mater Chem Phys., 101 (**2007**), 158–162
[27] X. H. Huang, Z. H. Chen, Scripta Mater., 54 (**2006**), 169–173
[28] H. Fujiki, K. Tomaru, I. Sakurai, A. Suzuki, K. Mita, US 2004/0054029 A1 (2006).
[29] Y. Mizuno, S. Taruta, K. Kitajima, J Mater Sci., 40 (**2005**) 1, 165–170
[30] M. R. Meshrama, N. K. Agrawala, B. Sinhaa, P. S. Misrab, J Magn Magn Mater., 271 (**2004**), 207–214
[31] M. H. Shams, S. M. A. Salehi, A. Ghasemi, Mater Lett., 62 (**2008**), 1731–1733